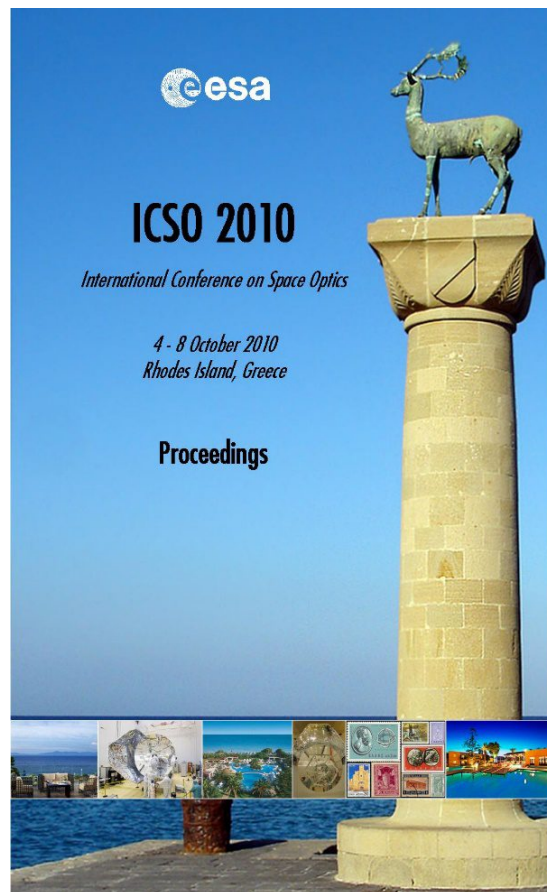


# International Conference on Space Optics—ICSO 2010

Rhodes Island, Greece

4–8 October 2010

*Edited by Errico Armandillo, Bruno Cugny,  
and Nikos Karafolas*



## ***First experimental demonstration of a temporal Hypertelescope operation***

*L. Bouyeron, S. Olivier, F. Reynaud, L. Delage*



International Conference on Space Optics — ICSO 2010, edited by Errico Armandillo, Bruno Cugny, Nikos Karafolas, Proc. of SPIE Vol. 10565, 105650E · © 2010 ESA and CNES  
CCC code: 0277-786X/17/\$18 · doi: 10.1117/12.2309192

## FIRST EXPERIMENTAL DEMONSTRATION OF A TEMPORAL HYPERTELESCOPE OPERATION

L. Bouyeron<sup>1</sup>, S. Olivier<sup>1</sup>, F. Reynaud<sup>1</sup>, L. Delage<sup>1</sup>.  
<sup>1</sup>Xlim, dept. photonique/IRO, France.

### I. INTRODUCTION AND CONTEXT:

#### A. Hypertelescope concept

High resolution Optical imaging instruments based on aperture synthesis have been developed over the last decades with the aim of reaching angular resolution in the nano radian range. These different instruments [1] take advantage of the property of the Zernike van Cittert theorem to recover the intensity distribution of the object from its spatial coherence analysis. With this method, the instrument can never select the light coming only from one of the pixels composing the full object because the measurements are being carried out on the Fourier spectral domain. For high-dynamic objects, such as a star + exoplanet system, this technique is limited since the information on the faint object is always mixed with the bright light emitted by the main source. Consequently, direct imaging is preferred and the analysis of the object is made easier in the image domain than in the Fourier spectrum one. Since the beginning of high resolution imaging, measurements have never been achieved both with a very high resolution in the range of nanoradian and a very high dynamics in the range of  $10^6$ . In order to meet this challenge, A. Labeyrie has proposed a solution called hypertelescope [2]. This new type of instrument solves the problem of the highly structured Point Spread Function (PSF) of a diluted array thanks to a pupil densification process. The PSF of a hypertelescope being sharp and smooth, it is possible to use the instrument for direct imaging. The image  $I$  equals the convolution of the object  $O$  by the  $PSF$ , looks like the object but with a limited resolution. Different versions of hypertelescopes have been proposed using field combination in the pupil plane [3] or pupil densification thanks to the use of monomode optical fibres [4].

#### B. Temporal version: principles and advantages

Parallel with the hypertelescope study promoted by A. Labeyrie, we have proposed a temporal alternative to the initial design using spatial classical optics (cf Fig.1). The main purpose of this new concept is to overcome some technical difficulties met with classical hypertelescope and to propose new functionalities. In reference [5] we have demonstrated that it's possible to design an hypertelescope by using temporal optical path modulation. In such configuration, we can retrieve the same imaging properties as for the first design using spatial pupil densification. To properly operate a temporal hypertelescope (THT), the optical path modulations have to be linear as function of time. It results in fringe frequencies  $\nu_i$  that have to be scaled to the phase slope  $(\alpha_i, \beta_i)$  of the classical hypertelescope [5].

In a classical hypertelescope, for a given telescope  $i$  and a given vertical position  $y_0$ , the phase variation  $\varphi_i$  observed in the image plane at  $(x, y_0)$  position is expressed as:

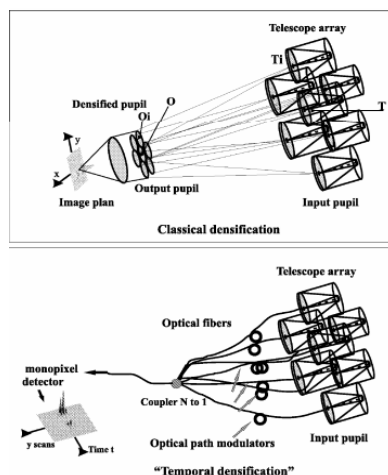


Figure 1 : Principle scheme of spatial and temporal hypertelescope

$$\varphi_i(x) = 2\pi(\alpha_i \cdot x + \beta_i \cdot y_0) = 2\pi\alpha_i \cdot x + \varphi_{i0}(y_0) \quad (1)$$

In a THT, the *spatial* linear phase modulation along the x axis is replaced by a *temporal* linear modulation inducing the same set of phase variations between the combined optical fields:

$$\varphi_i(t) = 2\pi\nu_i \cdot t + \varphi_{i0}(y_0) \quad (2)$$

By such way, the imaging capabilities of a spatial hypertelescope are fully recovered in the temporal configuration.

One of the main advantages of THT is the versatility for pupil reconfiguration. As long as the secondary pupil has to be homothetic to the telescope one, this functionality is very important for a ground based instrument or in space for a reconfigurable instrument. In addition to the "classical" imaging properties provided by a spatial hypertelescope, the THT allows to restrict the span of the field under study. For a nulled span, the temporal hypertelescope can operate as a spatial filter. In this case, it works as a nulling interferometer [6,7].

The breadboard and the related experimental results reported in the next paragraphs demonstrate the validity of this new concept.

## II. EXPERIMENTAL SETUP

### A. Technological options

Our experimental set-up (Fig.2) has been designed and implemented thanks to the different skills developed in our team since two decades [8-12]. Consequently, our THT experimental test bench uses optical fibres and couplers for the different optical functions to be implemented. However, note that the use of guided optic components is not mandatory for the implementation of a THT and a classical design with free space components could be chosen. This point remains minor as long as our paper is more focused on the demonstration of THT principle than on the technological aspect.

The following items give the general framework of our experimental study:

- The operating wavelength, all over this instrument, is  $\lambda=1,55\mu\text{m}$  to take advantage of the mature technologies of Telecom components.
- Light propagation from the entrance pupil to the detector is performed by monomode polarization maintaining fibres (panda fibres).
- All connections between the different components use FC/APC connectors to avoid parasitic back reflections.
- Our telescope array includes 8 apertures equivalent to a linear redundant configuration: the corresponding spatial frequencies sampling enables a convenient analysis of a complex linear object for a realistic experimental demonstration.
- The THT configuration has been optimized for imaging an unbalanced binary star with an high dynamic such as an exoplanet-star couple. For this purpose we will use the theoretical results reported in [13]. That implies a redundant spacing of the array and an optimized power distribution over the different telescopes to apodize the point spread function.

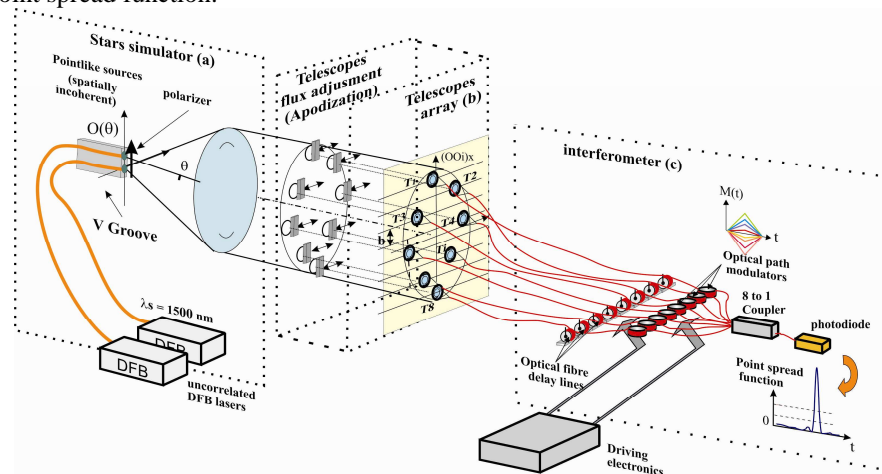


**Fig 2 : General scheme of our Temporal hypertelescope (THT) test bench. The main sub systems are described in detail in the text: The star simulator, the telescope array and the combining interferometer.**

B. *Star simulator*

The calibrated object is the first subsystem required for testing the imaging capability of a THT. For this first experimental demonstration, the selected “astronomical target” is a binary star with a convenient angular separation and adjustable dynamics.

For this purpose, the object consists of two tips of monomode Panda fibres glued on a V-groove. These monomode waveguides are fed by two independent Distributed Feed Back lasers (DFB) at the same wavelength and act as two incoherent point like sources. This way the object is spatially incoherent and the dynamics is controlled by adjusting the laser driving currents. A set of doublets and collimating lenses allows to provide an angular intensity distribution compatible with the spatial frequencies  $u$  sampled by our telescope array. In our experiment the angular separation  $O(\theta)$ , as seen by the telescope array, is  $23.75\mu\text{rad}$ . As our instrument is designed for a linear input polarization, a polarizing cube is inserted in the doublet spacing in order to select and to fix a linear vertical input polarization.

C. *Design of the telescope array*

The telescope array arrangement has to be carefully designed to fulfill the sampling criteria for a proper imaging analysis. As previously demonstrated [13], high dynamics imaging capability requires a redundant array configuration. Consequently, our telescope array must periodically sample the spatial frequency domain. The object dimension and the focal length of the collimator have to be determined by comparing the object spectrum and the spatial frequencies sampled by our instrument. The intensity  $I(A_t; y_0)$  observed in the image plane of the instrument is given by :

$$I(A_t, y_0) = \text{PSF} \otimes O(\theta) \quad (3)$$

where  $\otimes$  denotes the pseudo-convolution operator, PSF the point spread function of the instrument and  $O(\theta)$ , the object angular intensity distribution. In the Fourier domain, this relationship becomes a simple product:

$$\hat{I}(u) = T(u) \times \hat{O}(u) \quad (4)$$

where  $\hat{O}(u)$  is the object intensity spectrum and  $T(u)$ , the input pupil autocorrelation function. As shown in Fig. 7 the periodicity of the spatial frequencies sampled by the telescope array has to be compliant with the classical Shannon sampling criterium.

The smallest sampled frequency is related to the instrument field of view  $FV$  and the largest one determines the instrument resolution  $R$  :

$$FV = \frac{\lambda}{B_{\min}} \quad (5)$$

$$R = \frac{\lambda}{B_{\max}} \quad (6)$$

The telescope array resolution is related to the smallest observable detail on the object, whereas the field of view has to be adapted to the object’s overall size. This design trade-offs lead to the following THT bench characteristics:  $FV= 62\mu\text{rad}$ ;  $R=8.9\mu\text{rad}$ .

These values have been chosen to be compatible with the observation of our laboratory binary star characterized by a  $23.75\mu\text{rad}$  angular separation.

$$R < \theta_0 < FV \quad (7)$$

In order to image an unbalanced binary system with very high dynamics, the use of a set of suitable apodization coefficients will optimize the dynamics with a low reduction of resolution. On each aperture, the control of the intensity is achieved by means of mobile shutters actuated with high position accuracy according to the theoretical optimum distribution [13].

D. *The interferometric combiner*

The last part of the system is the optical field combiner mixing the contributions of the 8 telescopes. Each interferometric arm includes a fibre delay line and an optical path modulator [12]. The 8-fibre arms have been cut with a few mm accuracy in order to reduce the optical path differences as much as possible. The fibre delay lines allow to adjust the optical path with an accuracy of few  $\mu\text{m}$ . The fibre optical path modulators temporally reproduce the linear phase variation observed in the image plane of “classical” hypertelescopes (cf eq.1) and allow the fine residual optical path compensation. A National Instrument virtual instrument and a voltage generator have been developed to drive the piezoelectric actuators of the fibre optical path modulators. A set of high voltage amplifiers allows to reach a proper range of command

voltages. Experimentally, the optical path control is achieved with an optical path sensitivity lower than  $0.01\mu\text{m}$ .

The optical fields emerging from the 8 interferometric arms reach a 8 to one polarization maintaining (PM) coupler to achieve the interferometric mixing. At the output an InGaAs photodiode detects the interferometric signal that is recorded through a standard 12 bits ADC voltage acquisition system.

#### E. Cophasing system:

Unlike classical aperture synthesis instruments, Hypertelescope is a *direct* imaging instrument and its image quality is mainly limited by phase aberrations. Consequently, optical fields collected from each array aperture have to be cophase to obtain the best image quality.

To reach cophasing, we have chosen to use phase diversity technique combined with genetic algorithm (GA) (cf fig. 3).

##### a. Phase diversity technique

Phase diversity technique permit to define a phase quality criterion which is independent of the observed object geometry. It requires (at least) two images of the same object. The first image is a conventional image altered by unknown aberrations. Equation (3) gives:

$$I_1(A,t, y_0) = PSF_1 \otimes O(\theta)$$

with  $PSF_1$ , the classical instrument PSF limited by unknown phase aberrations. The second (and more) image, called diversity image, is obtain by introducing in the instrument an additional *known* aberration. Equation (3) gives:

$$I_2(A,t, y_0) = PSF_2 \otimes O(\theta)$$

where  $PSF_2$  is the instrument PSF when applying this additional aberration. Kendrick et al. propose in [14] four methods to obtain a phase quality criterion. We have chosen the first one which uses the M1 metric defined as:

$$\chi = \frac{\hat{I}_1(u)}{\hat{I}_2(u)} = \frac{T_1(u)}{T_2(u)} \quad (8)$$

where  $\hat{I}_1(u), \hat{I}_2(u), T_1(u), T_2(u)$  are the Fourier Transform of  $I_1(A,t, y_0), I_2(A,t, y_0), PSF_1$  and  $PSF_2$  respectively.

$\chi$  is independent of  $O(\theta)$  so it is the same regardless to the object geometry.

In our test bench, we use single-mode fibres and the object is totally unresolved by a single aperture. Therefore, phase aberrations are considered only as the piston errors.

The diversity image is achieved by *piston* diversity. On each interferometer arm we apply a known piston default with the system delay line. Finally, we compute the  $\chi$  parameter with the two object images. This reference value, called  $\chi_{ref}$ , is transmitted to the GA to compute the piston error on each interferometer's arm.

##### b. Genetic Algorithm

In a GA, a population of strings (called chromosomes) encodes the candidate solutions (called individuals) to an optimization problem. During the process, individuals will evolve toward better solutions. The evolution process starts from a population of randomly generated individuals. In each generation, individuals quality is evaluated by a function called fitness function. Multiple individuals are selected from the current population according to their fitness, and modified (recombined and possibly randomly mutated) to form a new population. The new population is then used in the next iteration of the algorithm [15].

In our system, the GA goal is to evaluate the piston bias to be corrected. This default could then be cancelled to cophase the system. We define an individual as a set of 8 (one for each interferometer arms) piston error values (chromosomes). Each population consists in 5 individuals. For each individual we compute the  $\chi$  corresponding parameter. The fitness function is define as:

$$F = \chi_{ref} - \chi \quad (9)$$

Individuals of the new population are generated by mixing and randomly mutating the chromosomes of the two best individuals (according to their fitness).

The GA gives its evaluation of the piston error after 30 iterations (few ms of computing time).

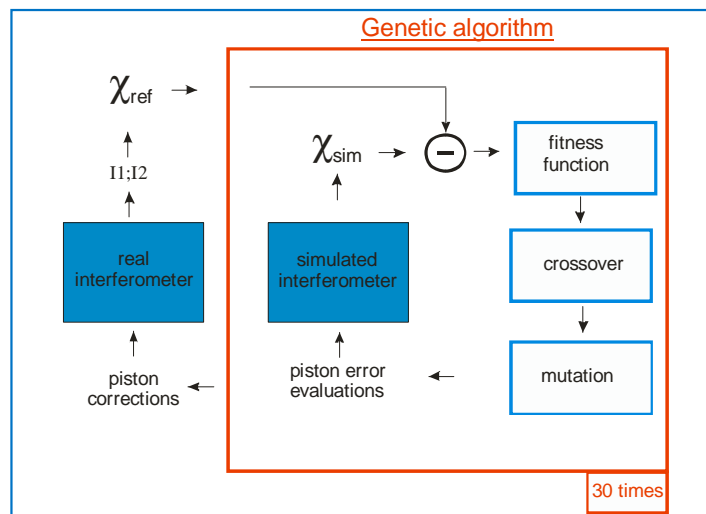


Fig. 3: cophasing system global scheme

III. EXPERIMENTAL RESULTS

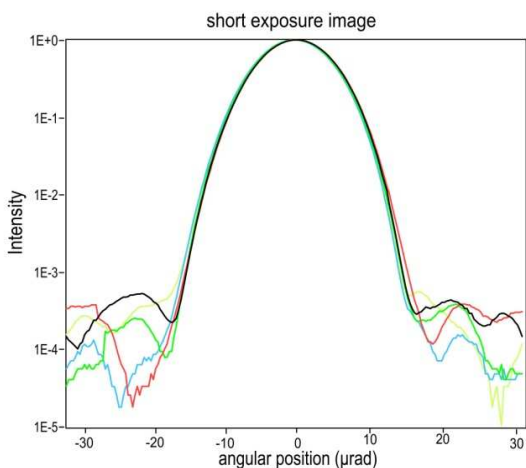


Fig 4 : short exposure image example

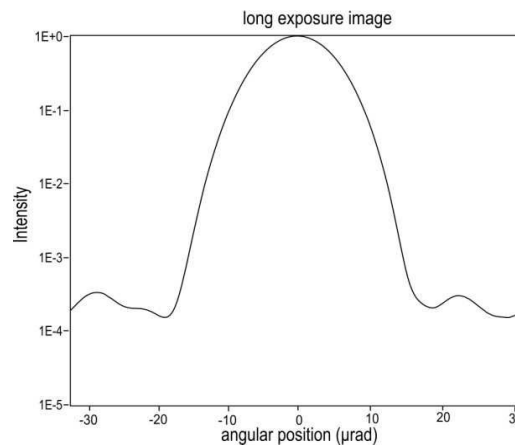


Figure 5 : long exposure image average of 1000 short exposure images during (~6 min)

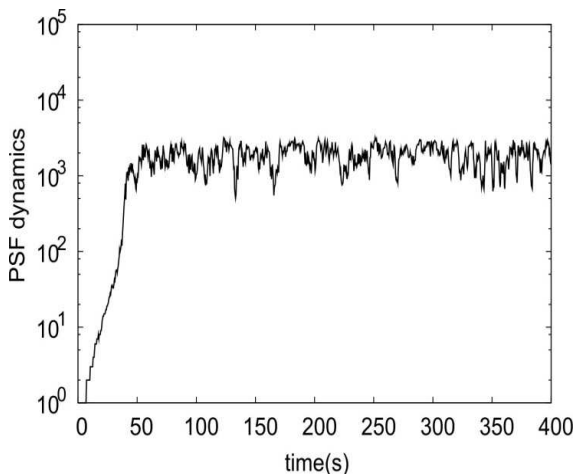


Figure 6 : experimental PSF dynamics versus time

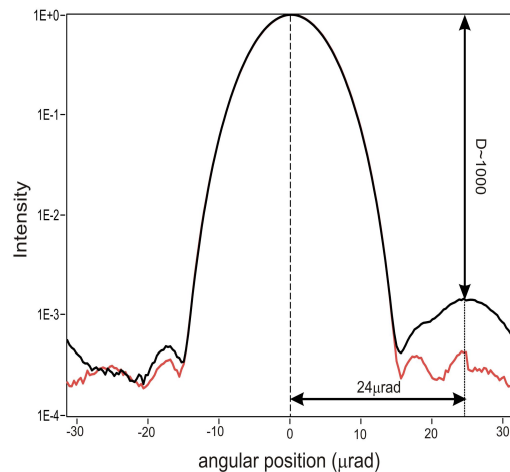


Figure 7 : Comparison between an unbalanced (dynamics ratio  $D= 1000$ ) binary star image (in black line) and a single star image (in red dots)

In order to calibrate the imaging capabilities of our instrument, we first experimentally characterized its point spread function. For this purpose, the telescope array has been illuminated by a plane wave using only one single point-like source (i.e. switching on only 1 source of the object). The voltage offsets of the electronic commands, which drive the optical path modulators, have been adjusted by our cophasing algorithm in order to increase the dynamics as much as possible. The first experimental results are shown in Fig. 4 and 5. Fig 4 shows short-exposure image examples and fig 5 shows the long-exposure image obtained by short-exposure images averaging. Experimental dynamics, observed with our breadboard, is in the range of 2000 (corresponding to a  $\sim\lambda/200$  cophasing) and as shown on fig.6, these results are stable over time thanks to our cophasing system. Such results have been obtained reliably and give a first indication on the THT imaging potential capabilities.

The second stage of our experimental investigation has been to obtain an image of the unbalanced binary star. For this purpose, the two fibre tips of the laboratory object receive the light from two different lasers which operate with the same wavelength. In this case, the two sources of the object are spatially incoherents. Adjusting the driving current allows to simulate any unbalanced binary source.

The experimental result are shown in fig.7. Each curve is obtained by one hundred short- exposure image averaging. The image in black exhibits a weak companion beside the main star. The 23.75 $\mu$ rad separation and a  $\sim 1000$  intensity ratio source characteristics are correctly recovered. The red curve shows the image obtained when the star's companion is switched off. Results are consistent with the theoretical convolution between the point spread function and the object intensity distribution. Consequently, the instrument imaging capabilities have been demonstrated.

#### REFERENCES

- [1] Lawson R., *Long Baseline Stellar Interferometry*, SPIE Milestone Series, Vol MS 139, Bellingham, 1997
- [2] Labeyrie A., A&AS, 118, 517, 1996
- [3] Vakili F., Aristidi.E., Abe L., Lopez B., A&A, 421, 147, 2004.
- [4] Patru F., Mourard D., Clausse J.M., et al., A&A, 477, 345, 2008.
- [5] Reynaud F., Delage L., A&AS, 465, 1093, 2007.
- [6] Bracewell R.N., Nature, 274, 780, 1978.
- [7] Leger A., Mariotti J.M., Mennesson B., Ollivier M., Puget, J.L., Rouan D., Schneider J., Icarus, 123, 249, 1993
- [8] Alleman J.J., Reynaud F., Connes P, Applied Optics, 34, 2284, 1995.
- [9] Simohamed L.M., Reynaud F, Pure and Applied Optics, 6, 37, 1997.
- [10] Huss G., Reynaud F., Delage L, Optics Communications, 196, 55, 2001.
- [11] G. Perrin, J. Woillez, O. Lai, et al., Science, 311, 194, 2006.
- [12] Olivier S., Delage L., Reynaud F., et al., Applied Optics, 46, 834, 2007.
- [13] Armand P., Benoist J., Bousquet E., Delage L., Olivier S., Reynaud F., European J. of Operational 195, 519, 2009.
- [14] Kendrick R. L., Acton D. S., Duncan A. L, A. Opt., 33(27), 6533., 1994.
- [15] Banzhaf W., Nordin P., Keller R., Francone F., *Genetic Programming – An Introduction*, Morgan Kaufmann, San Francisco, CA, 1998.